A&A 526, A143 (2011)
DOI: 10.1051/0004-6361/201014517

Astronomy & Astrophysics

Radio emission of SN1993J: the complete picture

II. Simultaneous fit of expansion and radio light curves

I. Martí-Vidal[1,2], J. M. Marcaide[2], A. Alberdi[3], J.C. Guirado[2], M. A. Pérez-Torres[3], and E. Ros[2,1]

[1] Max-Planck-Institut für Radioastronomie, Auf dem Hügel 69, 53121 Bonn, Germany
e-mail: imartiv@mpifr-bonn.mpg.de
[2] Dpt. Astronomia i Astrofísica, Universitat de València, C/ Dr. Moliner 50, 46100 Burjassot, Spain
[3] Instituto de Astrofísica de Andalucía (CSIC), C/ Camino bajo de Huétor 50, 18008 Granada, Spain

Received 26 March 2010 / Accepted 7 July 2010

ABSTRACT

We report on a simultaneous modelling of the expansion and radio light curves of the supernova SN1993J. We developed a simulation code capable of generating synthetic expansion and radio light curves of supernovae by taking into consideration the evolution of the expanding shock, magnetic fields, and relativistic electrons, as well as the finite sensitivity of the interferometric arrays used in the observations. Our software successfully fits all the available radio data of SN 1993J with a standard emission model for supernovae, which is extended with some physical considerations, such as an evolution in the opacity of the ejecta material, a radial decline in the magnetic fields within the radiating region, and a changing radial density profile for the circumstellar medium starting from day 3100 after the explosion.

Key words. acceleration of particles – radiation mechanisms: non-thermal – radio continuum: stars – supernovae: general – supernovae: individual: SN1993J – galaxies: individual: M 81

1. Introduction

We previously reported on an analysis of the complete set of available VLBI observations of SN 1993J (Martí-Vidal et al. 2011, hereafter Paper I). In that work, we confirmed the main results reported in Marcaide et al. (2009a) about an expansion curve that is dependent on the observing frequency. These results are not compatible with those published by other authors (Bartel et al. 2002), who claimed up to four different values of the expansion index, m (where the supernova radius is $R \propto t^m$ and t is the age after explosion, see Chevalier 1982a), corresponding to four different expansion periods. The interpretation of the data reported in Marcaide et al. (2009a) was very different: there is essentially one expansion index during the whole supernova expansion (in Paper I, we report however on two expansion regimes separated by an early *break time* at $t \sim 390$ days). Two explanations were then proposed in Marcaide et al. (2009a) for the different shell sizes found at different frequencies. On the one hand, an evolution in the opacity of the ejecta to the radio emission. This opacity was assumed to be maximum (i.e., 100%) at the lowest frequency (1.7 GHz) and slowly decrease in time at the higher frequencies, beginning about day 1500 after the explosion. On the other hand, a radial decay in the amplified magnetic fields within the emitting shell was also proposed. This profile in the magnetic-field distribution translates into a profile in the emission intensity, which (combined with the finite sensitivity of the interferometers used in the observations) can also help us to explain the expansion curve. In this paper, we quantify the effects proposed in Marcaide et al. (2009a) and Paper I by developing a new software capable to modelling simultaneously the expansion and radio light curves of SN 1993J.

The radio light curves of SN 1993J were previously modelled using several approaches: Weiler et al. (2002, 2007) used an analytical model to fit the data; Fransson & Björnsson (1998) and Pérez-Torres et al. (2001) simulated the evolution of the relativistic electron population inside the radiating region by taking into account the hydrodynamics of the shock evolution described in Chevalier (1982a) and the radiative cooling of the relativistic electrons; finally, Chandra et al. (2005) took into account synchrotron-ageing effects on the electron population. The claim of a steeper spectral index at high frequencies and late epochs made by Chandra et al. (2005) contradicted previous reports (Pérez-Torres et al. 2002a; Bartel et al. 2002) and was not confirmed by Weiler et al. (2007), who reported instead a flattening of the spectral index of the supernova at late epochs and all frequencies.

The remainder of this paper is structured as follows. In Sect. 2, we describe our new code for the simultaneous modelling of the SN 1993J radio light curves and expansion curve. In Sect. 3, we report on the final fitted model and describe the modifications (or extensions) of the Chevalier model (Chevalier 1982a,b) that were applied to our software to properly model the whole data set. In Sect. 4, we summarize our conclusions.

2. RAMSES: a simulator of the synchrotron emission from supernovae

To fit the radio light-curve data and, at the same time, fit the expansion curve of SN 1993J, we developed a new simulation code, RAMSES (Radiation-Absorption Modeller of the Synchrotron Emission from Supernovae). A detailed description of much of this model can be found in Martí-Vidal (2008). Some relevant aspects of the algorithms implemented in the program are also described in Appendix A of this paper. In this section, we summarize the main characteristics of RAMSES, which is

Table 1. Summary of fitted parameters, fixed parameters, and assumptions in the RAMSES model.

Fitted parameters		
$m_1 = 0.925 \pm 0.016$	$\bar{B}_0 = 65.1 \pm 1.6$ G	$n_0 = (6 \pm 0.9) \times 10^8$ cm^{-3}
$m_2 = 0.87 \pm 0.02$	$f_{\rm rel} = (5 \pm 0.5) \times 10^{-5}$	$T_l = (2.0 \pm 0.1) \times 10^6$ K
$t_{\rm br} = 360 \pm 50$	$p = -2.55 \pm 0.01$	$t_{\rm m} = 2500 \pm 100$ days
Assumptions and fixed parameters		
$s = 2$	$\bar{B}^2 \propto n_{\rm cs}\, V^2$	Changing ejecta opacity (vid. Fig. 7, left)
$t_0 = 5.3$ days	$n_{\rm rel}\, {\rm d}t \propto n_{\rm cs}\, V^2$	Non-uniform B (vid. Fig. 7, right)
$D_{\rm M\,81} = 3.63$ Mpc	$t_{\rm expl} = 1993$ March 28	

Notes. Details on the meaning of these quantities are given in Sect. 2 and Appendix A.

based on the work of Chevalier (1982a,b) and extended in several aspects. It assumes that: (1) the expansion is self-similar; (2) the radio-emitting region of the supernova is located between the contact discontinuity and the forward shock (the width of this spherical shell being 30% of the shell radius, see Marcaide et al. 2009a, and Paper I); (3) a given fraction, $f_{\rm rel}$, of the thermal electrons of the CSM are accelerated by the shock to relativistic energies and characterized by an energy distribution $\propto E^{-p}$, where p is the *energy index* of the electron population; (4) the electrons emit synchrotron radiation as they interact with an amplified magnetic field that fills the shocked circumstellar region; (5) the mean intensity of the magnetic field depends on the distance from the contact discontinuity; (6) the radius of the spherical surface defined by the contact discontinuity (although without considering the development of Rayleigh-Taylor fingers at this point) expands as $R \propto t^m$, where m is the *deceleration parameter* or expansion index ($m = (n-3)/(n-s)$); (7) during the expansion, the opacity of the ejecta to the radio emission may also evolve, and be different for different frequencies.

Our code RAMSES considers radiative cooling, inverse Compton scattering, and synchrotron self-absorption (SSA) in both the electron energy distribution and the radio emission. It generates synthetic images of the supernova that provide predictions of the expansion and radio light curves of SN 1993J. To determine the expansion curve, a high-pass filter of the flux density per unit beam is initially applied to the synthetic images, depending on the sensitivity of the VLBI arrays used in the observations. The Common-Point Method is then applied to the resulting images as in the case of real data (see Marcaide et al. 2009a) to obtain the model of the VLBI expansion curve.

Several parameters are fitted to the observed data by RAMSES (see Table 1 for a summary), including the: (1) density of CSM electrons, $n_{\rm csm}$, in the emitting region at a given (reference) epoch; (2) mean magnetic field intensity, $\bar{B}$ (i.e., average of the magnetic field intensity over the emitting region) at the same epoch; (3) energy index, p, of the electron energy distribution; (4) fraction, $f_{\rm rel}$, of the CSM electrons that are accelerated by the shock (i.e., the acceleration efficiency of the shock); (5) radial profile of the temperature of the unshocked CSM (which affects the free-free absorption, FFA, of the CSM, especially at early epochs, see Appendix A); and (6) mean lifetime, $t_{\rm m}$, of the relativistic electrons inside the supernova shell before they escape outside the emitting region. In Appendix A, we explain in more detail the meaning of these parameters. RAMSES assumes a power-law time evolution for the magnetic-field energy density and the energy density of the electrons at the shock, and generates the synthetic light curves and expansion curve. The model is then fitted to the observations by means of a least squares minimization (see Appendix A for more details). The expansion curve is parametrized in the same way as in Paper I (i.e., using two expansion indices, m_1 and m_2, separated by a break time, $t_{\rm br}$). Thus, our fits use 9 parameters. The "Best Fit" (SSA + FFA) model reported in Weiler et al. (2007) to fit the radio-light curves also had 9 fitting parameters, even though these authors did not include the expansion curve in their fits. In addition, we adopt several ad hoc assumptions about the evolution of the ejecta opacity, the profile of the CSM density, and the profile of the magnetic field, as described in the next few sections.

3. Simultaneous fit of expansion and radio-light curves

In Fig. 1, we show the fit of the RAMSES model to the radio light curves reported in Weiler et al. (2007) (top) and to the expansion curve reported in Paper I (bottom). In the fit, the structure index of the CSM was fixed to $s = 2$ and the CSM density was set to be 0 after day 3100 (see Sect. 3.2.4). For the reference epoch taken at 5.3 days after the explosion (when the radius of the contact discontinuity of the spherical shell is 10^{15} cm), we obtain a minimum reduced-χ^2 of 5.4 for the following values of the fitting parameters (see Table 1 for a summary): mean magnetic field, $\bar{B}$, 65.1 ± 1.6 G; post-shock circumstellar electron number density, $n_{\rm csm}$, $(6 \pm 0.9) \times 10^8$ cm^{-3}; acceleration efficiency, $f_{\rm rel}$, $(5 \pm 0.5) \times 10^{-5}$; energy index of the electron energy distribution, p, -2.55 ± 0.01; and a mean lifetime of the electrons inside the shell, $t_{\rm m}$, 2500 ± 100 days. The fitted $\bar{B}$, $n_{\rm csm}$, $f_{\rm rel}$, and p are similar to those reported by Fransson & Björnsson (1998). For values of s lower than 2 (i.e., $s = 1.6$–1.7), it is impossible to obtain satisfactory simultaneous fits to radio light curves and the expansion curve.

The best-fit model parameters for the expansion curve are: $m_1 = 0.925 \pm 0.016$, $m_2 = 0.87 \pm 0.02$, and $t_{\rm br} = 360 \pm 50$ days. The fitted m_2 is practically the same expansion index as that reported in Paper I for the shell sizes at 1.7 GHz (m_3 in that paper), and is close to the index reported in Marcaide et al. (2009a) (m_1 in that paper). The lower expansion index previously reported for the higher-frequency data (which corresponds to m_2 in Paper I and in Marcaide et al. 2009a) is modelled by RAMSES by considering several physical and instrumental effects (outlined in Marcaide et al. 2009a) that we describe in the next few subsections.

3.1. Particle-field energy equipartition

Our model assumes that the energy transmitted to the accelerated electrons by the shock at each time is proportional to the energy of the magnetic field, which is in turn proportional to the energy of the shock (see Table 1). However, the proportionality constants between these quantities are not fixed in our model, since we fit simultaneously the particle number density, the magnetic field (both at a reference epoch), and the acceleration efficiency

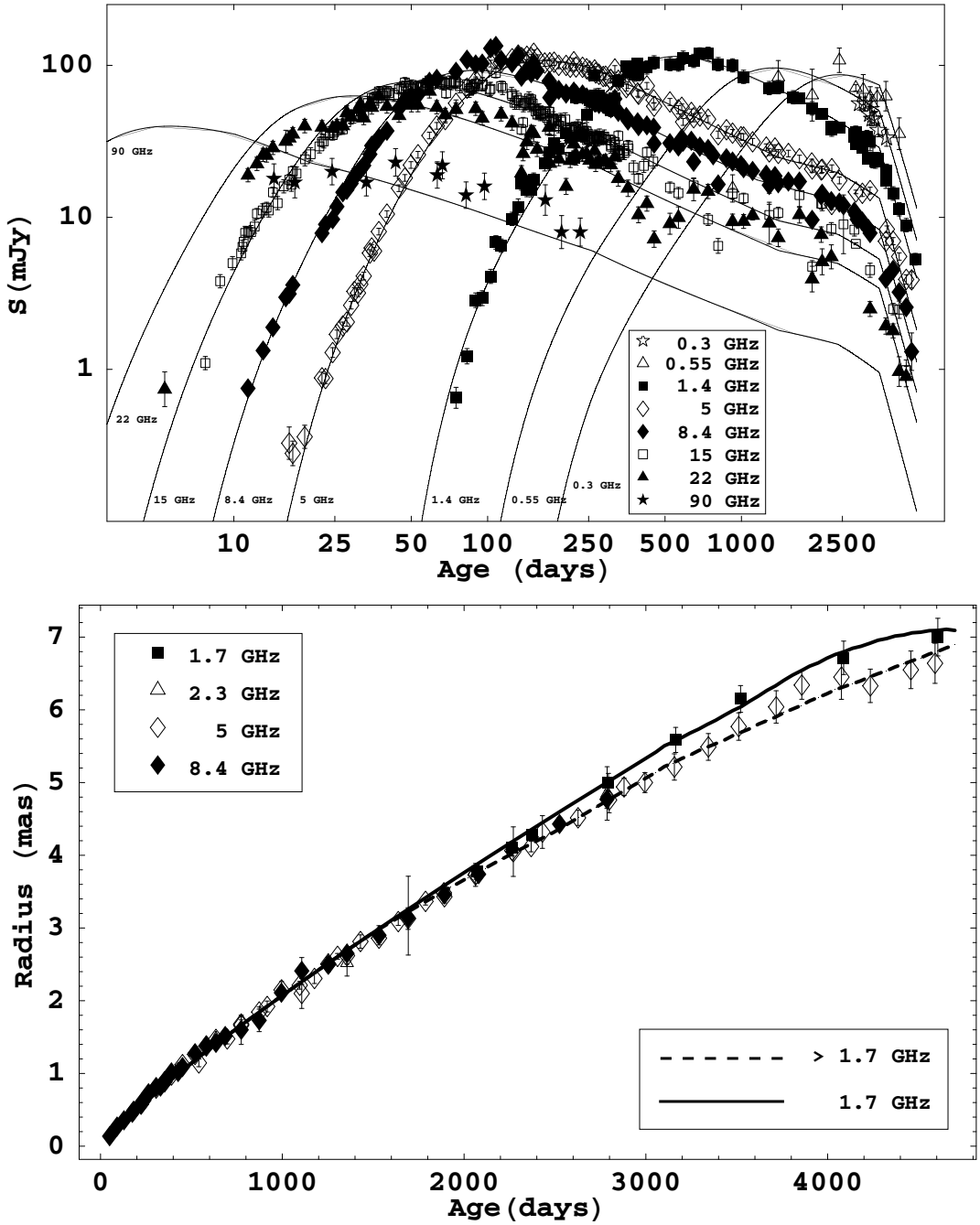

Fig. 1. *Top*, fit of RAMSES to the radio light curves reported in Weiler et al. (2007) up to an age of 4930 days. *Bottom*, simultaneous fit of RAMSES to the expansion curve reported in Paper I.

without any a priori covariance. Therefore, particle-field energy equipartition is not assumed in our model. However, we can estimate the level of energy equipartition between particles and fields from our best-fit model (an approach similar to that of Fransson & Björnsson 1998):

On the one hand, the energy density of relativistic electrons, relative to that of the thermal electrons in the shock, runs smoothly from $\sim 6 \times 10^{-5}$ at early epochs to $3\text{–}4 \times 10^{-4}$, at late epochs. If the acceleration efficiency of the ions were similar to that of the electrons, we would reach a rough level of equipartition between thermal and non-thermal particles in the shock.

On the other hand, the energy density of the magnetic field, relative to that of the thermal electrons, runs smoothly from 0.25 at early epochs to 0.06 at late epochs. In this case, the level of equipartition is not large, the magnetic field being a factor 2–4 below the equipartition value with the thermal shocked electrons.

Another way to analyze the level of equipartition is to compute the energy density of the magnetic field relative to that of the accelerated particles. In this case, the ratio runs from ~3000 at early epochs to ~170 at late epochs. Therefore, equipartition between magnetic field and relativistic particles is roughly obtained, again, provided that the efficiency in the acceleration of ions is similar to that of the electrons.

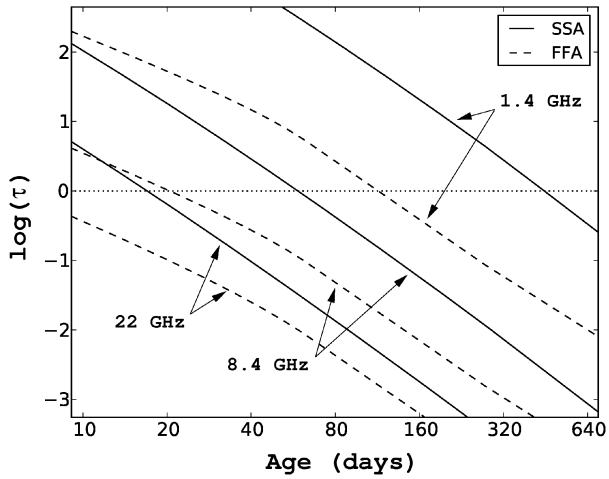

Fig. 2. SSA opacities (solid lines) and FFA opacities (dashed lines) versus time for a selection of frequencies.

3.2. Model of the CSM

3.2.1. FFA versus SSA

In Fig. 2, we show the SSA and FFA opacities computed with RAMSES in the optically-thick part of the light curves at 1.4, 8.4, and 22 GHz. It can be seen in the figure that SSA dominates versus FFA for all frequencies and epochs. The FFA evolution changes its slope at ∼80 days, because of the radial gradient of unshocked electron temperatures used in the model of the CSM (see next section and Appendix A). It can also be seen in Fig. 2 that, for each frequency, the opacity of SSA is $\tau \sim 1$ at roughly the same time as the light curve reaches its maximum (see also Fig. 1), as expected for SSA-dominated light curves. Chevalier (1998) studied the case of SSA-dominated light curves in radio supernovae and reported a relationship between the maximum flux-density at a given frequency, the supernova age at the maximum, and the mean expansion velocity of the shock. The mean expansion velocity estimated in this way is a lower bound to the true shock velocity when FFA is not negligible relative to SSA. The ratios of VLBI-inferred expansion velocities to those estimated using the relationship of Chevalier (1998) can be computed for several radio supernovae: this ratio is ∼2.6 for SN 1986J and SN 1979C (from the results reported in Pérez-Torres et al. 2002b; Bartel & Bietenholz 2003; and Marcaide et al. 2009b), 2.3−3.6 for SN 2004et (Martí-Vidal et al. 2007), and ∼2.5 for SN 2008iz (Brunthaler et al. 2010). However, for SN 1993J we find a much smaller ratio (∼1.5), which is indicative of a low FFA (or a high level of SSA compared to FFA), thus supporting the model here proposed for the SN 1993J radio emission.

We note that the minimum energy in the population of accelerated electrons (which we set to $m_e\,c^2$) affects the SSA opacity and, therefore, plays a role in the estimate of the electron number density, n_{csm}. If a low-energy cutoff is applied to the electron population, SSA decreases, although the effects of this cutoff are only significant at very early epochs, when the magnetic field is high and the electron energies corresponding to high critical frequencies are low. In the optically-thin part of the light curves, a low-energy cutoff does not change the emissivity, but when the source is optically thick a low-energy cutoff implies a larger source function (i.e., ϵ_ν/κ_ν) and therefore a larger fitted n_{csm} (to raise FFA in the optically-thick region and maintain the fit of the model to the observations). This, in turn, slightly decreases the fitted magnetic field, to fit the model to the observations in the optically-thin part of the light curves. In short, the use of a low-energy cutoff increases the importance of FFA relative to SSA (for instance, by a factor ∼2 if a cutoff of $10\,m_e\,c^2$ is applied), but the overall effects in the model light curves is very small.

3.2.2. Evolution of FFA opacity in the CSM

The flux-density evolution of a supernova in the optically-thick regime can provide detailed information on the radial density profile of the CSM. The opacity of the unshocked CSM to the radio emission is assumed to be produced by free-free interaction of the radiation with the thermal electrons that fill the ionized CSM. Therefore, a precise estimate of the CSM temperature is required to reliably model the CSM density profile using the radio light curves. By analysing the early X-ray and radio light curves of SN 1993J at several frequencies, Fransson et al. (1996) modelled a CSM radial density profile with an structure index $s \sim 1.7$, which is indicative of variable mass-loss rate for the precursor star. Similar results were found from the analysis of the late X-ray emission (Immleret al. 2001). However, Fransson & Björnsson (1998) were able to model the early radio light curves with $s = 2$ by adding cooling effects to the electron population and assuming a dependence of the CSM temperature on distance from the explosion centre, which maps into a radial dependence of the FFA. The use of this extra degree of freedom in the model resulted in a satisfactory fit to the radio light curves without assuming a variable mass-loss rate of the precursor star. In our work, we adopted the same approach as Fransson & Björnsson (1998). However, the added constraints provided by the expansion curve in the simultaneous fit made it difficult to obtain a good fit to the high-frequency (22 GHz) light curves at the earliest epochs (see Fig. 1). Our model overestimates the flux densities at 22 GHz in the optically-thick regime. However, the true radial profile of the CSM temperature could behave in many ways close to the explosion centre and/or evolve with time after the ionization produced by the initial flare from the supernova. This might explain the systematics in the 22 GHz residuals of the radio-light curve. A superior approach to using a model for the CSM opacity is possibly to estimate the opacity observationally, by comparing the measured flux densities to the opacity-free RAMSES predictions. In Fig. 3, we show our estimate of the evolution of the CSM free-free opacity at different frequencies. The flux density of the supernova was reproduced by the RAMSES model without FFA, multiplied by $\exp(-\tau)$, where τ is the opacity shown in Fig. 3.

We note that it is impossible to model the data shown in Fig. 3 using a simple model for the CSM temperature, as that described in Appendix A. The presence of inhomogeneities (i.e., clumps) in the CSM of a given radial distribution could help us to model the data. Indeed, the two earliest data points (the first one at 22 GHz and the second one at 15 GHz) in Fig. 3 do not follow the same general trend as the remainder of the data. The opacity at these two epochs is larger than expected from the backward extrapolation of the general trends. A possible explanation of these large opacities at very early epochs (earlier than 10 days after explosion) could be the presence of strong inhomogeneities (clumps) in the CSM close to the explosion centre. A rapid evolution of the CSM temperature to explain these large opacity changes is less realistic, since it would imply a sudden *re-heating* of the CSM during the first days after the shock breakout.

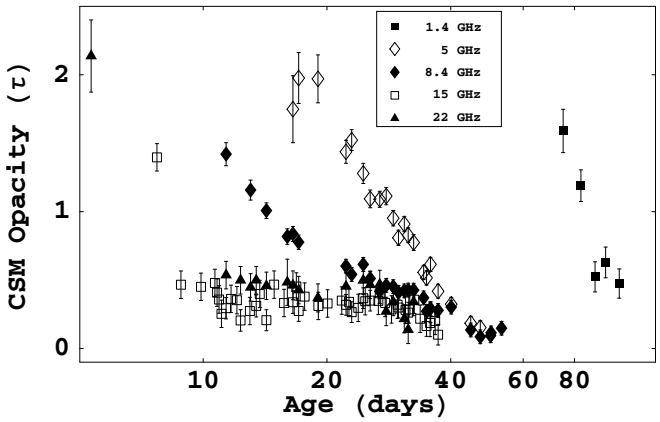

Fig. 3. Integrated line-of-sight free-free opacity of the unshocked CSM at several frequencies for the early phase of the supernova expansion, measured to be the ratio of observed flux densities to a SSA model.

3.2.3. CSM radial density profile

The break time fitted around day 360 after explosion may be due to an evolution in the structure index, n, of the ejected material, to a change in the structure index, s, of the CSM, or to a combination of both. In any case, if a value $s = 2$ is assumed after this early break, the parameter n after the break takes an effective value of 9.7, according to the Chevalier model. This relatively low value of n implies that there has been an enhancement of X-ray luminosity originating in the shocked ejecta region (although the X-ray emission could still be dominated by the circumstellar shock) given that the shock is more adiabatic and, therefore, its opacity becomes smaller (see Fransson et al. 1996). When Fransson et al. (1996) and Immler et al. (2001) estimated that $s \sim 1.6$–1.7 from their X-ray data, they did not consider the effect of a greater X-ray luminosity from the shocked ejecta due to $n \sim 10$. Mioduszewski et al. (2001) simulated radio images and the radio light curves of SN 1993J and also claimed that $s \sim 1.7$ provides the best fit to the data, although these authors did not take the electron radiative cooling into account. More recently, Nymark et al. (2009) reported on a fit to the SN 1993J X-ray data using a model with $s = 2$ and an X-ray emission dominated by the reverse shock. Chandra et al. (2009) were also successful in modelling the X-ray data using $s = 2$.

It is worth noticing that the wide fractional shell reported in Marcaide et al. (2009a) and Paper I (~30% of the outer radius) is incompatible with $s < 2$ in the frame of the Chevalier model (Chevalier 1982a), because for $s = 2$ this shell implies that $n \sim 6$ (see Table 1 of Chevalier 1982a). A lower value of s would imply an even lower value of n, which must be larger than 5 for a self-similar expansion (Chevalier 1982a). On the other hand, the combination of $n \sim 6$ and $s = 2$ translates into $m = 0.75$, a value much smaller than $m = 0.87$ (our fitted value after the break) although closer to the expansion index fitted to the 5 GHz data ($m \sim 0.8$, see Marcaide et al. 2009a; and Paper I), which, in our interpretation, does not describe the true supernova expansion. Could the similarity between the expansion index at 5 GHz and the theoretical value derived from a 30% fractional shell-width indicate that the true expansion curve (i.e., that corresponding to the forward shock) is traced by the high-frequency data? In this case, the evolution of the ejecta opacity would have been the opposite of that proposed in Marcaide et al. (2009a) and Paper I. That is, the ejecta would have been transparent to the radio emission at all frequencies and early epochs, and would have become increasingly opaque to the 1.7 GHz radiation after day 1500. We rule out this possibility, since in this case the fit to the radio light curves would be poorer and a value of n close to 6 (indeed, close to the limiting value $n = 5$ to keep the expansion self-similar) be too low. Baron et al. (1995), for instance, fitted ejecta density profiles with $n \sim 10$ for SN 1993J, based on non-local thermodynamic equilibrium (NLTE) synthetic spectra. The wide fractional shell reported in Marcaide et al. (2009a) and Paper I therefore remains unexplained[1].

In any case, we notice that it is difficult to discern whether s takes the value of 2 or smaller, since there is a tight coupling between the different variables that affect the evolution of the radiation produced by the circumstellar interaction of the expanding supernova shock. Our software satisfactorily fits the radio data assuming $s = 2$, but it also assumes that the evolution of the magnetic-field energy density (as well as the acceleration efficiency for the electrons) is proportional to the specific kinetic energy of the shock. A change in any of these (or other) assumptions of the model may affect our conclusions about the radial density profile of the CSM.

We note however that the conclusions extracted in the following subsections are independent of the real value of s.

3.2.4. Enhanced radial decline in the CSM density at late epochs

Weiler et al. (2007) found an enhancement of the flux-density decay rate after day ~3100. These authors fitted the enhanced decay rate using an *ad hoc* exponential factor with an e-folding time of ~1100 days, but noted that the same data can also be fitted (although worse) using a power-law decay with $\beta = -2.7$.

This decay takes place at all frequencies at the same time, leaving the spectral index of the supernova unaltered. These authors interpreted the exponential-like decay as being produced by a steeper, and fine-tuned, radial density profile of the CSM, beginning on day ~3100 after the explosion. In this section, we show that even an extreme drop in the density of the CSM cannot explain the observed fall-off in the flux density at all frequencies.

If all the electrons accelerated during the supernova expansion (and not only those that have just been accelerated after being affected by the shock, as it can be derived from Sect. 5.3 of Weiler et al. 2007) contribute to the radio emission, a change in the CSM density profile is not enough to explain such a rapid decay of the flux density. Cooling effects, and eventually the escape of electrons from the emitting region, can have important effects on the evolution of the supernova flux density at these late epochs, which we now consider in more detail.

We can obtain an upper bound to the flux-density decay rate after day 3100 by assuming that the CSM density profile approaches zero (or negligible values) from day 3100 onwards. In that case, the evolution of the expanding structure will no longer be self-similar. However, we can still derive the evolution of the expanding structure from the velocity fields given in Chevalier (1982a): the radial velocity of the shocked gas between the contact discontinuity and the forward shock is approximately equal to the expansion velocity of the contact discontinuity. If the supernova further expands into a negligibly dense CSM, the absolute (i.e., not fractional!) width of the shocked CSM region (i.e., from the contact discontinuity to the forward shock) will remain

[1] We note that even the narrower shell (25% of the outer radius) reported in Bietenholz et al. (2003) translates into a low value of n. In this case, we have $n \sim 7$ for $s = 2$. This estimate of n would be even lower if $s < 2$.

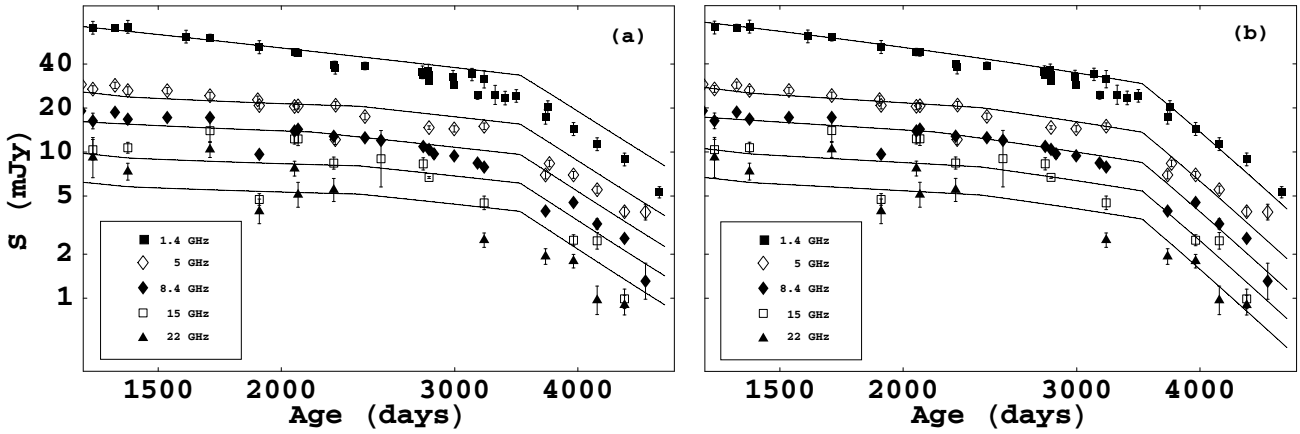

Fig. 4. Late radio light curves at several frequencies. Superimposed, RAMSES model obtained with a negligible CSM density after day 3100. **a)** Model with no escaping of the electrons from the emitting region. **b)** Model with a mean lifetime of the electrons inside the shell of 2500 days.

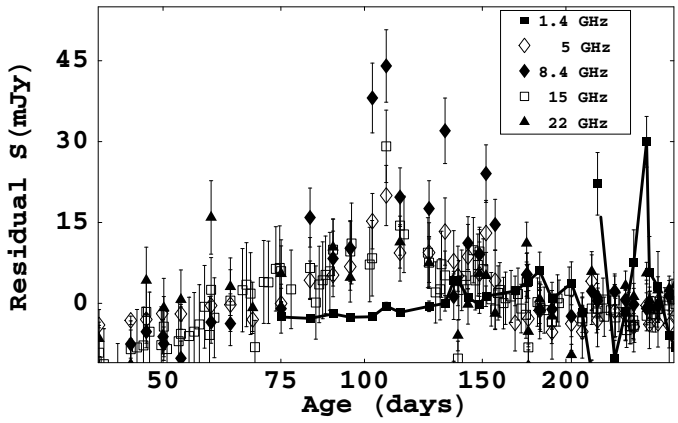

Fig. 5. Residual radio light curves from 40 to 250 days after explosion. The flux densities at 1.4 GHz are joined with lines for clarity.

constant, and the expansion velocity of the forward shock will be roughly equal to the expansion velocity of the contact discontinuity. Using these assumptions, we can compute an upper bound to the flux-density decay corresponding only to electron cooling (i.e., turning off the electron-escape term). Thus, from day 3100 onwards, we ensure that the total number of relativistic electrons inside the shell remains constant. We also assume the ratio of the particle energy density to the magnetic-field energy density to be constant (as in the Chevalier model). In Fig. 4a, we show the resulting simulated flux densities at late epochs superimposed on the observations reported in Weiler et al. (2007). We note that the flux-density decay rate predicted by RAMSES describes remarkably well the enhanced flux-density decay rate reported in Weiler et al. (2007), although with systematic slightly higher (around 10%) flux densities. These systematics would be lower if we were to shift the initial epoch of negligible CSM to earlier dates by 50−100 days. In other words, *radiative-cooling effects, alone, are able to model the late flux-density decay rate of the radio light curves*, provided the CSM density becomes negligible from day 3000−3100 onwards. A steep boundary in the CSM may be unrealistic, but it is conceivable that a rapid drop in the density is produced by the peculiarities in the onset of the stellar wind.

For a smoother density drop, cooling effects cannot describe, alone, the observed flux-density decay rate. In that case, other contributions to the flux-density decay rate must be invoked. The escape of the electrons from the radiating region is a natural way to enhance the flux-density decay rate. For instance, if the CSM structure index, s, were changed from 2 to, say, 4 on day 3100 (even disregarding the self-similar, standard interaction model scenario for radio supernovae), a mean lifetime of the electrons of about 1500 days (together with electron-cooling effects) could also explain the observations. We note that the mean lifetime of the electrons affects the electron evolution during the entire expansion, not only after day 3100. In the case of a negligible CSM after day 3100, adding electron escape with a relatively long mean lifetime (around 2500 days) decreases the flux densities predicted by the model without increasing so much the enhanced decay rate at late epochs, resulting in a better fit to the data (see Fig. 4b). This actually corresponds to our final choice for the simultaneous modelling of the radio light curves and the expansion curve of SN 1993J (see Sect. 3 and Fig. 1).

It is difficult to identify a model with the right combination of both factors (electron escape and enhanced radial density profile of the CSM), since both quantities are completely coupled. Therefore, the only clear conclusions we can reach at this point are: 1) an enhanced drop in the CSM density profile is needed to model the radio light curves after day 3100 and, depending on the amount of enhancement; 2) a finite mean lifetime of the electrons inside the radiating region may also be needed to explain the observations.

3.2.5. Flux-density flare at t ∼ 100 days

A zoom into Fig. 1 around $t = 100$ days uncovers a hint of excess emission from the supernova relative to the model predictions. This extra emission can also be seen in the residuals of the model reported in Weiler et al. (2007). In Fig. 5, we show the residuals around day 100 the after explosion. We note that the extra emission is detected at 5, 8.4, 15, and 22 GHz, but not at 1.4 GHz. This extra emission of about 30–40 mJy (i.e., increase in total flux density of the supernova by ∼40%) lasted about 50 days. It was, therefore, a relatively large flux-density flare of the supernova. It is remarkable that the flare was not detected at 1.4 GHz. The source was optically thin at the other frequencies, so the intensity was roughly proportional to the electron number density. In contrast, according to our model, the source was optically thick to the synchrotron radiation at 1.4 GHz during the flare. Thus, the intensity at that frequency was roughly

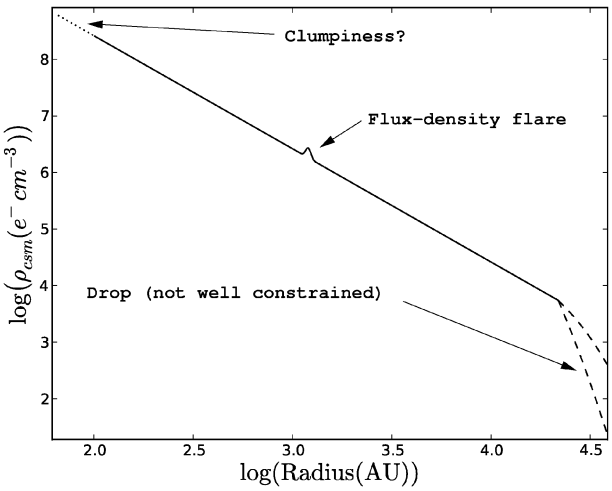

Fig. 6. Squematic representation of CSM density vs. distance to the explosion centre.

equal to the source function (j_ν/κ_ν), which, avoiding the small effects of radiative cooling on the electron population, is independent of the electron number density (e.g. Pacholczyk 1970). Therefore, a straightforward interpretation of Fig. 5 is that the number density of shocked CSM electrons suddenly increased by about 40% around day 100 after the explosion (supernova radius of ∼1150 AU). We note that an increase in the magnetic field when modelling the flare cannot explain why it did not take place at 1.4 GHz. Unfortunately, the supernova structure was not well resolved with VLBI at those early epochs and it is not possible to correlate the flare shown in Fig. 5 with any change in the emission structure of the supernova.

In Fig. 6, we show a schematic representation of the CSM radial density profile inferred from the whole analysis reported here. On the one hand, for radial distances below ∼100 AU there is evidence of clumpiness, based on the larger CSM opacities computed from the observations (see Fig. 3). At a distance of ∼1150 AU, a flare in the light-curve residuals provides evidence of an overdensity in the CSM. Finally, for radial distances larger than 21 000 AU, the CSM drops faster than $\propto r^{-2}$, the exact profile not being very well determined and dependent of the electron escaping used in the model.

3.3. Evolution of the ejecta opacity

As proposed in Marcaide et al. (2009a), a changing ejecta opacity (which would be different for different frequencies) helps to explain the wavelength effects found in the expansion curve. In Paper I, we confirmed those wavelength effects. We implemented the opacity effects suggested in Marcaide et al. (2009a) into the RAMSES model, although they are difficult to parametrize. Since the ejecta opacity can evolve in many different ways, several possibilities were tested. In Fig. 7, we show the final model selected for the ejecta opacity evolution. This model does not have any theoretical justification, but the true opacity should not be very different from the model proposed here. This model optimally fits all the radio data. In principle, one would expect that the evolution of the ejecta opacity must not be the same at all frequencies higher than 1.7 GHz. It seems more plausible that the opacity at higher frequencies should begin to decrease before those at lower frequencies. However, the data is not good enough to allow for such a careful modelling of the ejecta opacity.

The opacity at frequencies higher than 1.7 GHz linearly decreases from 100% (on day 1500) to 0% (on day 2500), but remains constant at this frequency. This decrease in the ejecta opacity can explain the wavelength effects reported in the expansion curve of the supernova, but can also explain a slight increase in the SN 1993J flux densities observed after day ∼1500 in the 8.4 GHz data (and, to a lower degree, also in the 5 GHz data) reported by Weiler et al. (2007). In Fig. 9, we show the flux-density residuals corresponding to the model used by Weiler et al. (2007) around day 1500 after explosion. In Fig. 10, we show the residuals of RAMSES for the same time range. We note that the RAMSES residuals are typically half of those of Weiler et al. (2007), and even ∼5 times smaller for some data points. The effect of opacity evolution can also be seen in the measured spectral indices. In Fig. 8, we show the spectral indices reported by Weiler et al. (2007) between 1.4 and 5 GHz, comparing them with the model proposed by these authors and our model obtained with RAMSES. In the time window between 500 and 5000 days after the explosion, the systematic offsets between data and the model proposed by Weiler et al. can clearly be seen. Instead, the RAMSES model predicts remarkably well the evolution of the spectral index for all epochs, including the flattening beginning at an age ∼1000 days (Pérez-Torres et al. 2002a; Bartel et al. 2002).

In Marcaide et al. (2009a) and Paper I, we reported a fitted ejecta opacity of 80% for all epochs and frequencies. This result might seem to be in conflict with the model proposed here for the evolution of the ejecta opacity. However, we also noted then that the ejecta opacities reported were too noisy for extracting any robust information about the possible evolution and/or spectral dependence of the ejecta opacity. Therefore, the value of 80% reported there for the opacity should be taken as an approximate, average, value.

3.4. Radial drop of the magnetic field

Inside the shell it is also difficult to parametrize a radial drop in the magnetic field. After extensive testing, we chose the following model to characterize the drop of B, as a function of distance, D, from the contact discontinuity

$$B(D) = B_0(a\,D^2 + b\,D + c), \quad (1)$$

where the parameters a, b, and c are chosen so that, for a fractional shell width of 0.3, B_0 is the mean magnetic field intensity of the shell and the intensity at the forward shock is half the intensity at the contact discontinuity (see Fig. 7).

Marcaide et al. (2009a) pointed out that if the flux density per unit beam decreases, the shell size estimate will be biased towards a smaller value, provided the magnetic field drops radially in the shell (see their Sect. 7.1.2). Thus, the exponential-like decrease in flux densities after day 3100, combined with a magnetic field structure similar to that given in Eq. (1), should translate into progressively biased estimates of the shell size, and therefore an increase in the (observed) deceleration of the expansion curve. If we include radial drops in the magnetic field steeper than that corresponding to Eq. (1) (such as a linear or a concave-like decay), we obtain poorer fits to the expansion curve. Therefore, we conclude that the radial drop in the magnetic field inside the shell must be smooth. In Fig. 11, we compare the expansion-curve residuals obtained with a uniform magnetic field inside the shell (a) with those for the magnetic-field

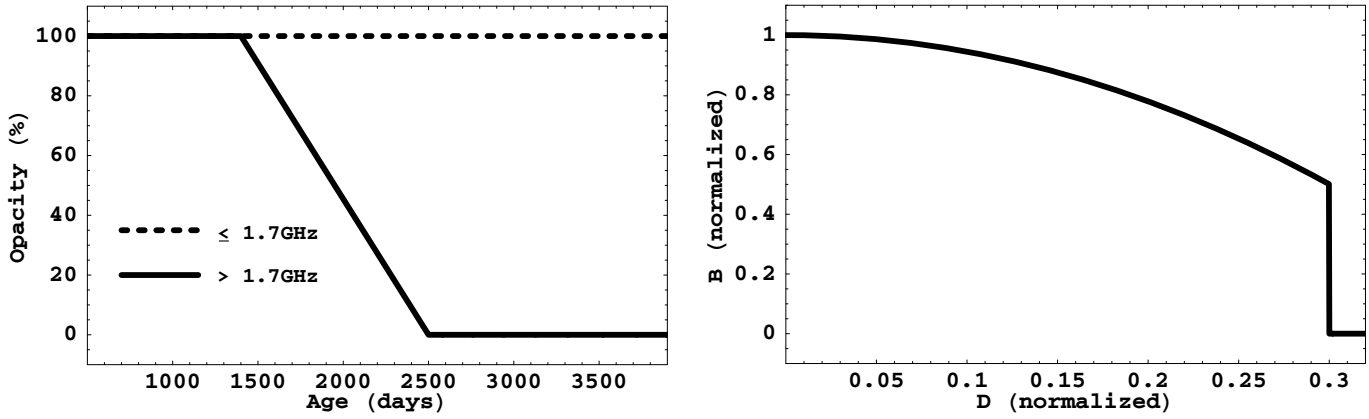

Fig. 7. Ad hoc assumptions of the RAMSES model, based in Marcaide et al. (2009a) and Paper I. *Left*: evolution of the ejecta opacity used in the RAMSES simulations; 100% means maximum opacity (total blockage of the radiation from behind the ejecta); 0% means no ejecta opacity. *Right*: mean amplified magnetic field (normalized to the magnetic field at the contact discontinuity) as a function of distance from the contact discontinuity (normalized to the shell radius).

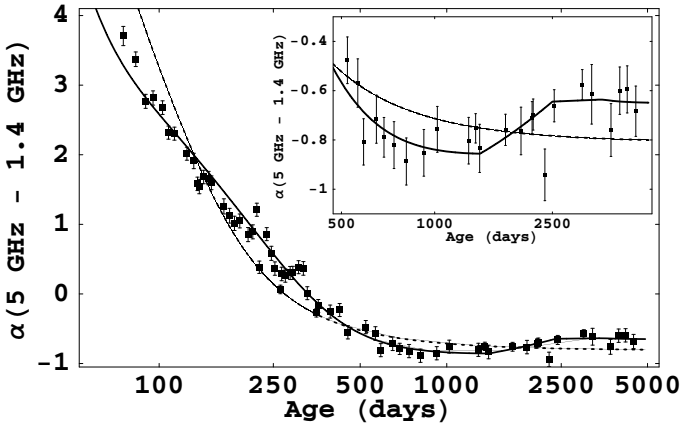

Fig. 8. Observed spectral indices between 1.4 and 5 GHz reported by Weiler et al. (2007). Dashed line, best-fit model reported by Weiler et al. (2007). Continuous line, best-fit obtained with the RAMSES model. Inset is a blow up from day 500 to 5000.

structure given by Eq. (1) and shown in Fig. 7. It can be seen that the residuals for the latest VLBI epochs are more accurately fitted using the radially-decaying magnetic field.

We note however, that the conclusions extracted from this section are based on noisy images (from the latest epochs at which the supernova could be barely imaged). Therefore, these conclusions should be considered with caution.

4. Conclusions

We have developed software to simultaneously model the VLBI expansion curve and the radio light curves of supernova SN 1993J. This software takes into consideration the evolution of the magnetic field energy density and the hydrodynamic evolution of the expanding shock, as well as the relativistic acceleration of CSM electrons as they interact with the supernova shock. All these processes have been implemented following Chevalier (1982a,b). Our software also accounts for the radiative cooling of the electrons, as well as SSA and inverse Compton scattering. The escape of electrons from the radiating region is also considered.

We have modelled the whole radio-data set of SN 1993J (radio light curves and expansion curve) using one single model.

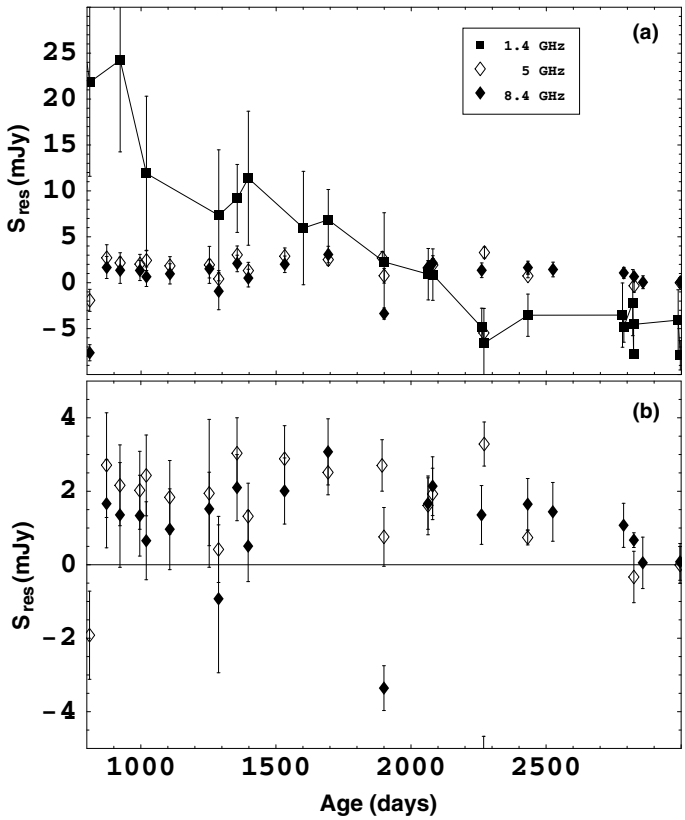

Fig. 9. Residuals of the SN 1993J flux densities between days 1000 and 3000 after explosion, using the model of Weiler et al. (2007): **a)** all the residuals (1.4 GHz residuals have been joined with a solid line for clarity); **b)** zoomed, the residuals at 5 and 8.4 GHz (the solid line now marks the zero mJy level).

We have considered a changing opacity of the supernova ejecta to the radio emission and a radial decay in the magnetic field within the radiating region. The structure index of the CSM is set to $s = 2$ up until day 3100 after the explosion. From that day onwards, a higher value of s, or even a negligibly dense CSM, is required to model the radio light curves. In the case of a negligibly dense CSM, cooling effects, alone, are able to predict the exponential-like flux-density drop reported by Weiler et al. (2007). When the CSM is not negligible after day 3100, a finite

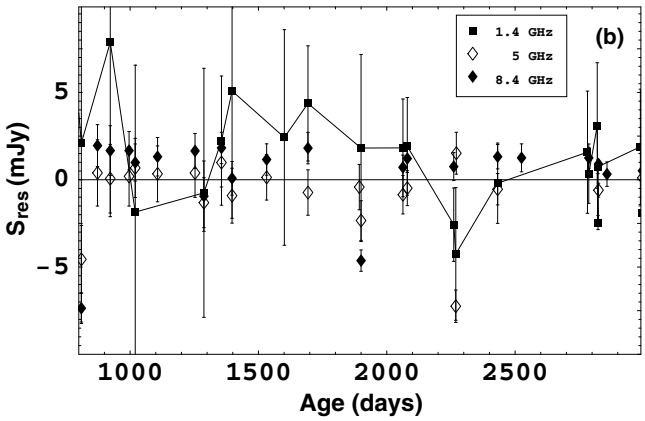

Fig. 10. Same as in Fig. 9a, but with the residuals obtained with the RAMSES model.

mean lifetime of the electrons inside the emitting region is also needed to model the late radio light curves. We also find, at all frequencies apart from 1.4 GHz, an unmodelled increase in the flux density of the supernova around day 100 after the explosion. This increase represents ∼40% of the total flux density of the supernova at these epochs. We suggest that this sudden increase in the flux density may be caused by an increase in the density of the shocked CSM electrons around day 100.

In our model, the ejecta opacity remains constant at 1.7 GHz, but changes at the other frequencies from 100% (at day 1500 after explosion) to 0% (at day 2500). This evolution of the opacity explains the effects found in the expansion curve and is also able to explain some effects found in the radio light curves (hence, in the evolution of the spectral indices).

We also found evidence of a radial drop in the magnetic field inside the radio shell. When combined with the enhanced flux-density decay rate of the radio light curves at late epochs, this drop explains the enhanced deceleration found in the expansion curve of the latest VLBI observations at all frequencies.

Acknowledgements. I.M.V. is a fellow of the Alexander von Humboldt Foundation in Germany. The National Radio Astronomy Observatory is a facility of the National Science Foundation operated under cooperative agreement by Associated Universities, Inc. The European VLBI Network is a joint facility for European,Chinese, South African and other radio astronomy institutes funded by their national research councils. Partial support from Spanish grant AYA 2005-08561-C03-02 is ackwnowledged. A.A. and M.A.P.T. acknowledge support by the Spanish Ministry of Education and Science (MEC) through grant AYA 2006-14986-C02-01, and by the Consejería de Innovación, Ciencia y Empresa of Junta de Andalucía through grants FQM-1747 and TIC-126. The National Radio Astronomy Observatory is a facility of the National Science Foundation operated under cooperative agreement by Associated Universities, Inc. The European VLBI Network is a joint facility of European,Chinese, South African and other radio astronomy institutes funded by their national research councils.

Appendix A: The RAMSES model

A.1. Equation of the electron evolution

As implemented by Fransson & Björnsson (1998), we simulated the relativistic electron population using the equation of continuity in energy space

$$\dot{N}(E,t) = -\nabla_E(\dot{E}N(E,t)) + S(E,t) - L(E,t), \quad (A.1)$$

where $N(E,t)$ is the number of electrons that fill the radiating region with energies between E and $E + \mathrm{d}E$ at time t, $S(E,t)$ is the source function accounting for the continuum acceleration of CSM electrons by the shock, $L(E,t)$ takes into account the possible escaping of electrons from the emitting region, and $\dot{E}$ represents the energy loss (or gain) of an electron with energy E at time t. In the following subsections, we explain each term of Eq. (A.1) in more detail.

A.2. Energy losses of the electrons

Our software considers several terms for the computation of energy losses of the relativistic electrons (negative terms for $\dot{E}$). These terms are the expansion of the relativistic gas (which results in $\dot{E} \propto E/t$) and radiative processes (synchrotron, Coulomb, and inverse Compton; see Pacholczyk 1970).

In the case of synchrotron losses, we have $\dot{E} \propto \bar{B}_\perp^2 E^2$, where $\bar{B}_\perp^2$ is the mean of the square of the perpendicular component of the magnetic field to the (random) trajectories of the electrons.

Coulomb losses are modelled with $\dot{E} \propto (f_\mathrm{a} + \log E)E$, for free-free processes, and with $\dot{E} \propto (f_\mathrm{b} + \log E)$, for processes related to the ionization of the medium (f_a and f_b are constants that can be computed from the density of hydrogen in the medium, see Pacholczyk 1970).

We also included losses due to the inverse Compton effect, which only affects the earliest radio light curves at the highest frequencies. In this case, $\dot{E} \propto J\,E^2$, where J is the photon density inside the radiating region. The photon-density estimates used in our modelling were taken from Fransson & Björnsson (1998, see their Fig. 6).

A.3. Energy gain of the electrons

Once the electrons have been accelerated by the shock, their main process of energy gain is SSA, since the probability of being re-accelerated is very low (the acceleration efficiency of the shock $\sim 10^{-5}$, see fitted value of F_rel in Table 1). To compute the effect of self-absorption in the electron energy distribution, we must take into account possible radial variations in the amplitude of the magnetic field in the shell, especially for the emission frequencies for which the optical depth is close to 1. It can be shown (see Martí-Vidal 2008) that the expression to use in this case is

$$\left(\dot{E}N\right)_\mathrm{ssa} = E^2\nabla_E\left(\frac{n(E)}{E^2}\right)\int\int \frac{K_s}{\nu^2} I_\nu(S)F(x)\,\mathrm{d}S\,\mathrm{d}\nu, \quad (A.2)$$

where the integral over S is the integral over the radiating region, and the integral over ν is that over all the synchrotron emission frequencies. $I_\nu(S)$ is the synchrotron emission intensity at the point S of the source and at frequency ν. The factor $n(E)$ is the density of electrons with energies between E and $E + \mathrm{d}E$ in the point S of the source. This equation is a generalization of that used by Fransson & Björnsson (1998), but can be applied to magnetic fields with generic amplitude distributions inside the source. The amplitude of the magnetic field, as a function of its position S, appears implicitly in x and K_s (the definitions of x, K_s, and $F(x)$ can be seen in Pacholczyk 1970).

A.4. Source of electrons

The source function of electrons depends on energy and time. We assumed an expression similar to that one used by Fransson & Björnsson (1998)

$$S(E,t) = F_\mathrm{rel}F_\mathrm{nor}N_0(R/R_0)^{-s}(V/V_0)^2E^{-p},$$

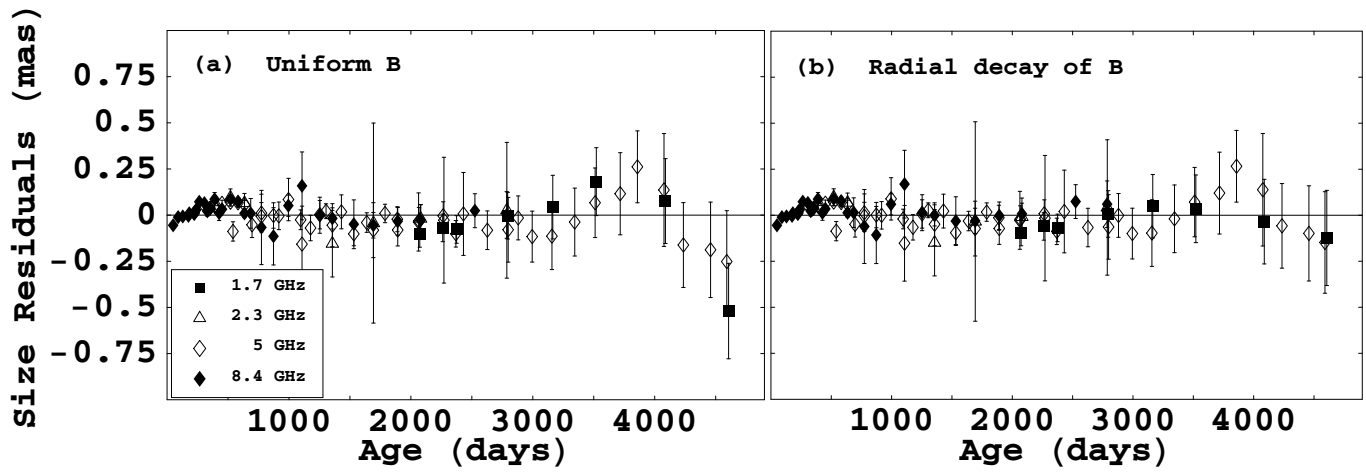

Fig. 11. Residuals of the expansion curve modelled with RAMSES using a uniform **a)** and a radially-decaying **b)** magnetic field inside the shell. The shape of the radial decay of the magnetic field is given by Eq. (1) and shown in Fig. 7.

where $F_{\rm rel}$ is the fraction of electrons of the recently-shocked CSM that have been accelerated, N_0 is the electron density at a reference epoch (when the radius of the supernova shell was R_0 and the expansion velocity was V_0), R is the radius of the shell, V its expansion velocity, and $F_{\rm nor}$ is a normalization factor. This normalization factor scales the amplitude of an electron population distribution given by $N(E) \propto F_{\rm rel}N_0$ into a population of relativistic electrons with an energy distribution given by $N(E) \propto E^{-p}$, in such a way that the number of electrons is conserved.

The factor $(V/V_0)^2$ is included to make the acceleration efficiency of the shock proportional to its specific kinetic energy. This proportionality has been found to more accurately describe the electron acceleration, according to Fransson & Björnsson (1998).

A.5. Escaping of electrons from the emitting region

Electrons could escape from the emitting shell, either towards the unshocked CSM or into the region of expanding ejecta. The escaping of electrons from the emitting region was assumed to be independent of the electron energies. All the electrons have velocities close to the speed of light, and the effect of the magnetic-field pressure inside the emitting region should be similar for all the electrons. These two reasons make the probability of escaping from the shell roughly equal for all electrons. Therefore, the expression used to model the escaping of electrons is

$$L(E,t) = N(E,t)/t_{\rm m}, \tag{A.3}$$

where $t_{\rm m}$ is the mean lifetime of an electron inside the radiating shell.

A.6. Electron evolution and radio emission

Numerical integration of Eq. (A.1) is performed semi-implicitly (see Martí-Vidal 2008). This equation can be written as $\dot{N} = f(N, \nabla_E N, E, t)$, where f is a functional that depends on $N(E)$, E, and t. If we apply a binning of $N(E,t)$ in energy and time[2], such that $N_{k,i}$ is the electron number at energy E_k and time t_i, we can approximate Eq. (A.1) by

$$\frac{N_{k,i+1} - N_{k,i}}{t_{i+1} - t_i} = \frac{1}{2}\left(f + (N_{k,i+1} - N_{k,i})\nabla_N f\right). \tag{A.4}$$

Knowing the electron population at time t_i (i.e., knowing $N_{k,i}$ for all k), it is possible to compute the new population at time t_{i+1} (i.e., $N_{k,i+1}$ for all k). However, care must be taken when computing $\dot{E}N(E,t)$ in Eq. (A.1), especially the term related to SSA, for which an accurate estimate of the intensity distribution of synchrotron radiation inside the shell is needed.

Once $N_{k,i+1}$ was obtained, we computed the emission intensity at all the desired frequencies, and transmitted the result through a filter that takes into account the opacity due to the unshocked CSM electrons. This opacity can be estimated using the equation (e.g., Pérez-Torres 1999)

$$\tau_\nu = C_{\rm f}^{-2}\,\frac{0.17}{\nu^2}\int_R^\infty n_{\rm cs}(r)^2\,T(r)^{-3/2}\left(1+0.13\,\log\left(\frac{T(r)^{3/2}}{\nu}\right)\right){\rm d}r \tag{A.5}$$

given in the cgs system, where $C_{\rm f}$ is the compressing factor of the shocked CSM density relative to the unshocked CSM density. This factor is ∼4 (e.g., Dyson & Williams 1980), $T(r)$ is the temperature of the unshocked CSM medium as a function of distance to the supernova explosion centre. RAMSES uses the same temperature profile used by Fransson & Björnsson (1998)

$$T(r) = {\rm Max}\left(T_{\rm l} \times \left(\frac{R_0}{r}\right)^{\delta}, T_{\rm c}\right), \tag{A.6}$$

where $T_{\rm c} = 2 \times 10^5\,K$, $\delta = 1$, and $T_{\rm l}$ is a fitting parameter.

Afterwards, the opacity-corrected flux densities were used to generate the synthetic radio light curves and the VLBI images. A cut-off was then applied to the VLBI images according to the sensitivity of the interferometric arrays. Finally, the Common-Point method (see Marcaide et al. 2009a; and Martí-Vidal 2008) was applied to generate the synthetic expansion curve at all frequencies.

A.7. Fitting procedure

When the synthetic radio light curves and expansion curve have been generated, the software compares them with the observations and computes the corresponding χ^2. Then, new values of

[2] We apply a logarithmic binning in energy and time to optimize the accuracy of the numerical integration.

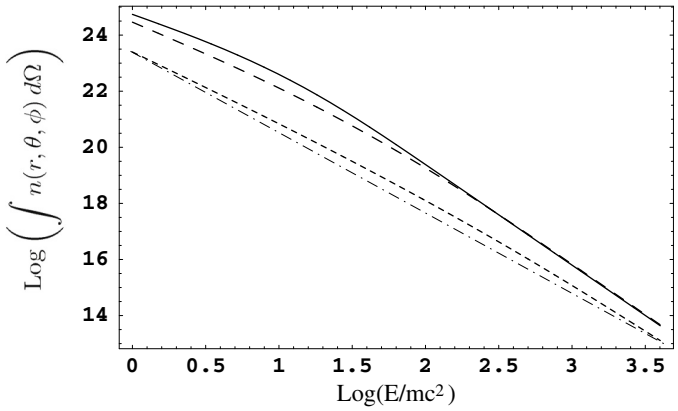

Fig. A.1. Energy distribution of the solid-angle integral of an electron population simulated with RAMSES, computed in the forward shock. The continuum line is the population at 10 days after explosion. The long-dashed line is the population at 100 days. The short-dashed line is the population at 1000 days. The dot-dashed line is a straight line, plotted for visual aid.

the simulation parameters are computed to minimize the χ^2. This step is performed using the SIMPLEX algorithm (e.g., Nesa & Coppins 1981). The whole process is iterated until convergence of SIMPLEX.

A.8. Test of RAMSES

The integration code of RAMSES was tested in several ways. The conservation of the number of electrons after applying Eq. (A.4) was tested. On the one hand, at low energies ($E \rightarrow mc^2$) the particle number is not well conserved, since $\dot{E}N(E,t)$ was computed using expressions that are only valid in the relativistic regime. However, the low-energy region of the electron population is full of thermal (i.e. non-accelerated) electrons, which dominate the distribution and, moreover, those electrons do not contribute to the synchrotron emission. Therefore, this lack of conservation of the non-relativistic electron population is not crucial in our simulations. On the other hand, the upper limit to the energy distribution used in the simulations ($10^4\, mc^2$) produces a small generation of electrons at the highest-energy boundary of our integration window. Nevertheless, this effect is very small (of the order of 10^{-6} times the source function $S(E,t)$ at those energies). We also tested the degree of convergence of the solutions as a function of the number of bins in energy and time spaces. Setting 3000 time steps (between days 2 and 4900 after explosion) and 1000 bins in energy space (between 1 and 10^4 Lorentz factors), we obtain results that differ only ~0.1% from the results obtained using twice the number of bins.

The electron population obtained also evolves as it is expected if we consider the energy gains and losses, as well as the injection and escaping of electrons. In Fig. A.1, we show an example of the evolution of an electron population obtained after a RAMSES run. At 10 days after explosion, a small *bump* is seen at $E \sim 10\, m\, c^2$, due to the energy gain produced by SSA (i.e., electrons with this energy emit with a peak frequency for which the mean opacity is $\tau \sim 1$). Later, radiative losses dominate, and the spectral index tends to increase 1 (in absolute value) at higher frequencies and decrease 1 (in absolute value) at lower frequencies. Both effects can be appreciated in Fig. A.1, with the help of the straight line also shown in the figure.

References

Baron, E., Hauschildt, P. H., Branch, D., et al. 1995, ApJ, 441, 170
Bartel, N., & Bietenholz, M. F. 2003, ApJ, 591, 301
Bartel, N., Bietenholz, M. F., Rupen, M. P., et al. 2002, ApJ, 581, 404
Bietenholz, M. F., Bartel, N., & Rupen, M. P. 2003, ApJ, 597, 374
Brunthaler A., Martí-Vidal I., Menten K. M., et al. 2010, A&A, 516, A27
Chandra P., Ray A., & Bhatnagar S., 2004, ApJ, 612, 974
Chandra, P., Dwarkadas, V. V., Ray, A., et al. 2009, ApJ, 699, 388
Chevalier, R. A. 1982a, ApJ, 258, 790
Chevalier, R. A. 1982b, ApJ, 259, 302
Chevalier, R. A. 1998, ApJ, 499, 810
Dyson, J. E., & Williams, D. A., 1980, Physics of the Interstellar Medium (New York: Wiley)
Fransson, C., & Björnsson, C.-I. 1998, ApJ, 509, 861
Fransson, C., Lundqvist, P., & Chevalier, R. A. 1996, ApJ, 461, 993
Immler, S., Aschenbach, B., & Wang, Q. D. 2001, ApJ, 561, L107
Marcaide, J. M., Martí-Vidal, I., Alberdi, A., et al. 2009a, A&A, 505, 927
Marcaide, J. M., Martí-Vidal, I., Perez-Torres, M. A., et al. 2009b, A&A, 503, 869
Martí-Vidal, I. 2008, Ph.D. Thesis, University of Valencia, Spain
Martí-Vidal, I., Marcaide, J. M., Alberdi, A., et al. 2007, A&A, 470, 1071
Martí-Vidal, I., Marcaide, J. M., Alberdi, A., et al. 2011, A&A, 526, A142 (Paper I)
Mioduszewski, A. J., Dwarkadas, V. V., & Ball, L. 2001, ApJ, 562, 869
Nymark, T. K., Chandra, P, & Fransson, C. 2009, A&A, 494, 179
Nesa, W., & Coppins, R. 1981, Linear Programming and Extensions (New York: McGraw-Hill)
Pachoolczyk, A. G. 1970, Radio Astrophysics (San Fransisco: Freeman)
Pérez-Torres, M. A. 1999, Ph.D. Thesis, University of Valencia, Spain
Pérez-Torres, M. A., Alberdi, A., & Marcaide, J. M. 2001, A&A, 374, 997
Pérez-Torres, M. A., Alberdi, A., & Marcaide, J. M. 2002a, A&A, 394, 71
Pérez-Torres, M. A., Alberdi, A., Marcaide, J. M., et al. 2002b, MNRAS, 335, L23
Weiler, K. W., Panagia, N., Montes, M. J., & Sramek, R. A. 2002, ARA&A, 40, 387
Weiler, K. W., Williams, C. L., Panagia, N., et al. 2007, ApJ, 671, 1959